Photovoltaic Frequency-Watt Curve Design for Frequency Regulation and Fast Contingency Reserves

Jay Johnson, *Member, IEEE*, Jason Neely, *Member, IEEE*, Jarod Delhotal, and Matthew Lave, *Member, IEEE*
Sandia National Laboratories
Albuquerque, NM
jjohns2@sandia.gov

***Abstract*—When renewable energy resources are installed in electricity grids, they typically increase generation variability and displace thermal generator control action and inertia. Grid operators combat these emerging challenges with advanced distributed energy resource (DER) functions to support frequency, and provide voltage regulation and protection mechanisms. This paper focuses on providing frequency reserves using autonomous IEC TR 61850-90-7 pointwise frequency-watt (FW) functions that adjust DER active power as a function of measured grid frequency. The importance of incorporating FW functions into a fleet of photovoltaic (PV) systems is demonstrated in simulation. Effects of FW curve design, including curtailment, deadband, and droop, were analyzed against performance metrics using Latin Hypercube Sampling (LHS) for 20%, 70%, and 120% PV penetration scenarios on the Hawaiian island of Lanai. Finally, to understand the financial implications of FW functions to utilities, a performance function was defined based on monetary costs attributable to curtailed photovoltaic production, load shedding, and generator wear. An optimization wrapper was then created to find the best FW function curve for each penetration level. It was found that in all cases, the utility would save money by implementing appropriate FW functions.**

***Index Terms* -- advanced inverter functions, grid-support functions, advanced inverters, smart DER, frequency regulation.**

I. Introduction

In June 2015, Hawaii passed a renewable portfolio standard (RPS) bill that required Hawaiian utilities to generate 100% of their energy from renewable sources by 2045 [1]. In order for the Hawaiian Electric Industries to meet this requirement, an assortment of energy technologies must be implemented, including installation of energy storage systems and activation of advanced grid-support functions in PV and other DER inverters.

Advanced DER functions have been gaining acceptance in Europe and the United States as a cost-effective tool for improving grid stability. Grid codes around the world have been adding grid-support requirements for PV and Energy Storage Systems (ESS) [2]-[6], major activities are creating interoperability standards to communicate with the devices [7]-[9], and international research programs are creating advanced DER testing protocols [10]-[13].

Frequency-watt (FW) implementation is required in distributed energy resources in many European countries [2] and is included as an optional function in California Electric Rule 21 [3]. Deployment of distributed active power controls to provide ancillary services including regulation and primary contingency reserves is well studied in the literature [14]-[18]. The active power headroom for PV inverters is derived from operating off the maximum power point (MPP). In the grid codes, this curtailment is defined as a percentage of the nameplate power of the DER; thus, the curtailment is only active for the part of the day for which available solar power exceeds the curtailment level. In laboratory experiments of the response time of advanced grid-support functions, the inverters were found to rapidly respond in approximately 0.25 seconds when decreasing power—though the inverter response can be multiple seconds when increasing output to near maximum power [19].

This work explores the influence of FW function parameters on multiple performance and economic figures of merit (FOMs) for the small island grid on Lanai, Hawaii. This evaluation is done at current and future (speculative) penetration levels. Given the large number of parameter permutations, Latin Hypercube Sampling (LHS) [20] was used to design simulation experiments to investigate the relationship between FW parameters and FOMs using (a) General Electric's Positive Sequence Load Flow (PSLF) software and (b) a simplified dynamic model in MATLAB with full day (sunrise to sunset) irradiance profiles. The former was used to simulate transient events during *N*-1 contingencies while the latter provided aggregate performance data over a diurnal solar cycle. Finally, an economic study was performed on selection of FW parameters to minimize total cost attributed to energy loss due to curtailment, generator wear, and risk of blackout.

II. LANAI GRID MODELS

Lanai is a 140.5 square mile Hawaiian island with approximately 3,200 residents in 1,150 households, living mostly in Lanai city. The power system includes a 10.4 MW diesel power plant with ten generators, three 12.47 kV distribution circuits, and the 1.2 MW La Ola PV power plant [21]-[22]. The peak load of the island is approximately 6 MW. It is noted that the diesel power plant does not energize all generators; in this study two, three or four generators were

This work was supported by the U.S. Department of Energy SunShot program under Award Number 29092. Sandia National Laboratories is a multi-program laboratory managed and operated by Sandia Corporation, a wholly owned subsidiary of Lockheed Martin Corporation, for the U.S. Department of Energy's National Nuclear Security Administration under contract DE-AC04-94AL85000.

online depending on the PV penetration scenario being simulated.

A. Frequency-Watt Function

While there are a range of timing and hysteresis differences between grid codes, the FW curve is either defined through parameters, such as in the German VDE-AR-N 4105 [6], or with a pointwise method, such as in the IEC 61850-90-7 FW22 function, shown in Fig. 1. In this report, we define pointwise FW curves but have made a number of assumptions to reduce the degrees of freedom:

1. The FW curve is constructed of four points.
2. The deadband is centered on nominal frequency.
3. No slope through nominal frequency
4. The slope of the FW curve is the same for over and under-frequency.
5. GP_1 is at full rated power and GP_4 is at zero power.

With these assumptions, the FW curve can be fully defined using three easy-to-understand parameters:

1. curtailment, with range 0-100%
2. deadband, with range 0-2 Hz
3. droop, with range 0.001-2.0 Hz/100%

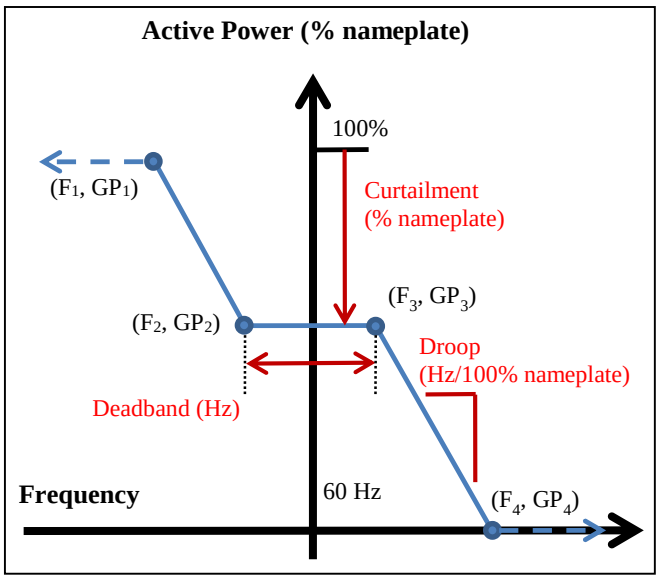

Fig. 1. Defining the pointwise FW curve with three parameters.

Although the function response time was found to be different in hardware experiments for increasing and decreasing power [19], the function response was modeled in this study to be symmetrical with the same time constant for increasing and decreasing power output.

B. PSLF Model

General Electric's PSLF software was used to model two grid event scenarios (a generator outage and a line-to-ground fault on a distribution line feeding a well pump) with three PV penetration levels (20%, 70% and 120%) using irradiance data from three different times of day (early morning, late morning, and midday). In this work, penetration level was defined as installed PV nameplate power divided by peak load. To account for the time-varying PV power availability, ground-measured irradiance time series were scaled with the Wavelet Variability Model (WVM) [23]-[26] to create PV power values that were fed into the 240 second PSLF simulations. The PSLF models were validated against data collected at the Lanai La Ola PV plant for the 20% penetration case [19].

For the higher penetration scenarios, additional PV generators were simulated at Lanai city (residential) as well as at resort and industrial locations with time-shifted irradiance profiles resulting from an assumed northerly wind direction [19]. Within this model, in the 20% case there were:

- three PV systems (each PV system aggregates multiple inverters) totaling 1.2 MW, and
- four diesel generators.

In the 70% case, there were:

- eight PV systems totaling 4.2 MW, and
- three diesel generators.

And in the 120% case, there were:

- thirteen PV systems totaling 7.2 MW, and
- two diesel generators.

It is noted that two generators are still necessary in high penetration cases so that *N*-1 contingency is satisfied.

To illustrate the benefits of FW functions, a FW implementation is compared in simulation to simple inverter curtailment (no frequency support). Both scenarios consider a 70% PV penetration scenario with a late morning irradiance profile. The FW curve was defined with $GP_2 = GP_3 = 50\%$, 0.1 Hz deadband, and droop = 1.25 Hz/100% nameplate. The curtailed case was set to 50% of nameplate. Fig. 2 shows the simulated electrical generator speed for the *Lanai 7* diesel generator following loss of *Lanai 5* diesel generator (rated at 1.2 MW) at t = 120 sec. The FW and curtailment scenarios exhibit similar response to PV variation between t = 50 and 100 seconds, but following the loss of the *Lanai 5* generator, a sizable improvement is seen in frequency response with the FW implementation.

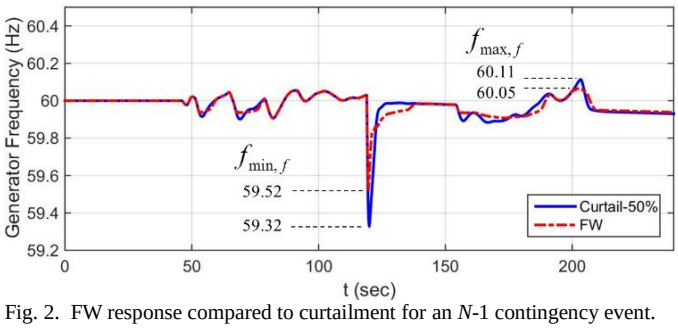

Fig. 2. FW response compared to curtailment for an *N*-1 contingency event.

C. Simplified Lanai Power Model

The simplified power model was created to evaluate the FW function performance during day-long, non-contingency scenarios. Three days of irradiance data were used with the WVM to predict the PV power during 20%, 70%, and 120% penetration scenarios. The days were selected based on previous research [21] to capture the full range of PV ramp rates located at La Ola.

- December 7th, 2010 – Least Variable
- September 3rd, 2010 – "Average" Variability
- November 4th, 2010 – Most Variable Total Day

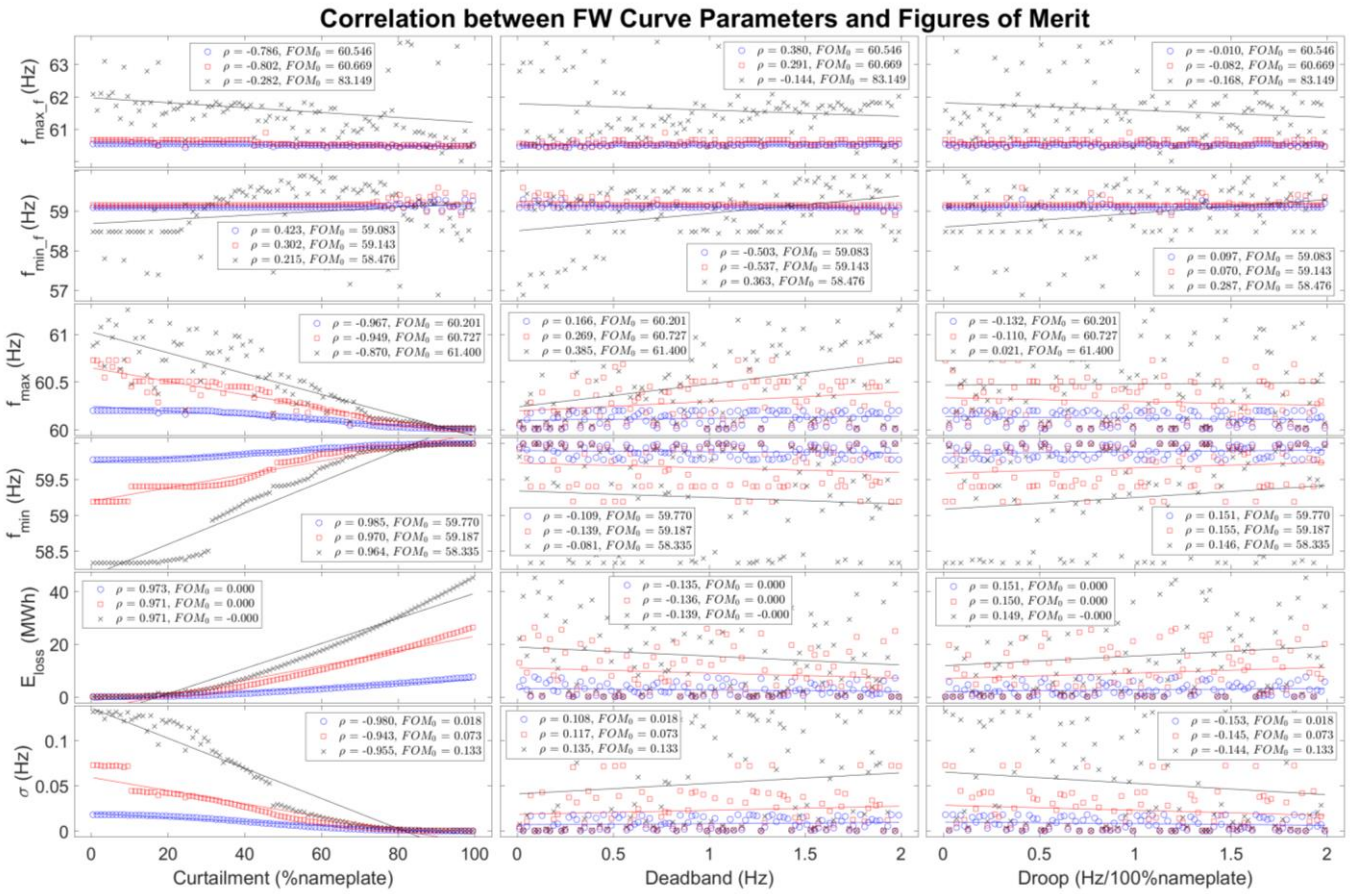

Fig. 3. LHS results illustrating the sensitivity of six figures of merit (y-axes) to FW parameters (x-axes) for 20% (blue), 70% (red) and 120% (black) penetration.

A dynamic model of the Lanai power grid was created based on diesel generator characteristics, including inertia, damping and speed governor controls as well as variable PV power computed using the WVM. The load, however, was assumed constant. This model used a 4th-order Adams-Bashforth integration method with a 0.001 second timestep to simulate grid dynamics based on the generator inertia, damping, droop and isochronous control. The model is described and compared to Lanai frequency data in [19].

III. Latin Hypercube Sampling

Latin Hypercube Sampling enables the intelligent design of simulation experiments and was used to compare the influence of the three FW curve parameters on a number of different metrics (i.e., figures of merit) from the simplified power model and PSLF simulations. The FOMs were selected based on performance of the system for non-event operation subject to variable PV generation and during fault scenarios:

- The maximum (f_{max_f}) and minimum (f_{min_f}) grid frequency measured at the power plant for the six different PSLF scenarios (two fault types and three times during the day).
- The average PV energy loss, E_{loss}, for the three days with different irradiance values.
- The absolute minimum (f_{min}), absolute maximum (f_{max}), and average standard deviation (σ) of the Lanai grid frequency for the three simulation days.

The LHS results for 100 FW curves are shown in Fig. 3 for the three penetration cases. The FW curves were the same for each of the three penetration scenarios so direct comparisons can be made across the different penetration levels. The 100 LHS-generated curves are shown in Fig. 4. The Pearson correlation coefficient, ρ, is displayed for each of the FW parameters with respect to each FOM to help determine the influence of the FW parameter on the metric. The FOM_0 value is the result without the FW function. A first order linear regression is also shown to illustrate the relationship between the FW parameters and the FOMs. The following general comments can be made from the LHS analysis:

- Curtailment has the strongest influence on the FOMs; in particular, E_{loss} is highly dependent on the curtailment setting ($\rho_{20\%}$=0.973, $\rho_{70\%}$ = 0.971, $\rho_{120\%}$ = 0.971).
- As curtailment increases, the frequency range for the non-event and fault cases decreases. This is expected in the 24-hour simulations since energy imbalance (load minus generation) is caused only by PV variability, i.e., the load is fixed in the model.
- In the PSLF simulations, the largest curtailment provides the greatest headroom for the PV to respond to the loss of generation event.
- Deadband and droop have less effect on the FOMs.
- An increasing deadband tends to widen the frequency deviation during non-event and fault cases.
- While a minor influence, for the majority of cases, steeper slope (smaller droop) led to more aggressive compensation and decreased frequency deviation.

- The ability of the FW function to reduce frequency fluctuations increases with greater PV penetration, as evidenced by the larger FOM ranges.

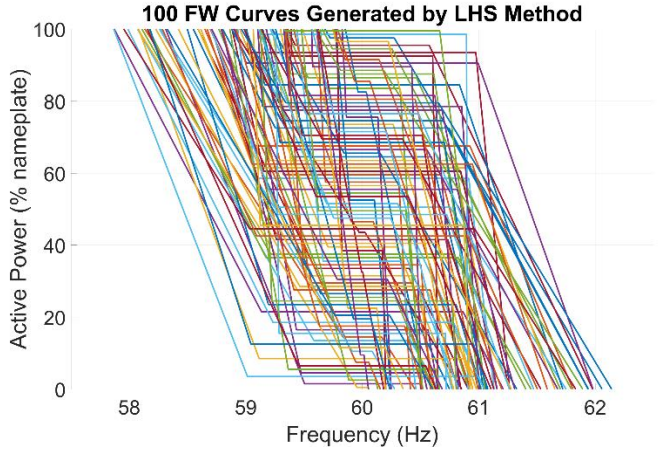

Fig. 4. The 100 LHS-generated FW curves used in the simulations.

IV. Cost of Frequency-Watt Implementation

Utility companies and grid operators would like to implement optimal FW curves for each penetration scenario based on the implementation costs. Any number of cost functions could be created depending on the tradeoff preferences of the utility or system operator which produce different optimal FW curves. We do not consider the financial implications of increasing PV penetration levels from indirect costs or externalities (public health and environmental impacts), but rather, compare costs directly associated with and without the FW function. By employing renewable energy resources as frequency regulation and primary contingency reserves, the lost revenue from PV production is offset by the reduced service interruption costs and reduced lifecycle costs attributed to generator wear; three costs were selected:

1. The average revenue lost from FW curtailment for three days, calculate from the price of electricity and E_{loss},
2. The cost of blackouts, the consumer interruption costs based on f_{min_f}.
3. The operations and maintenance (O&M) costs for the synchronous generators associated with grid frequency fluctuations, σ.

Taking a holistic view of grid operations, the PV owners should be compensated by the utility for their participation in regulation and contingency reserve, so the lost revenue from FW curtailment is transferred to the utility, and the total utility cost is:

$$Cost = \sum_i \left[P_i \cdot \bar{f}_i(FOM_i) \right] = P_1 \cdot \bar{f}_1(E_{loss}) + P_2 \cdot \bar{f}_2\left(f_{\min\_f}\right) + P_3 \cdot \bar{f}_3(\sigma) \quad (1)$$

where P_i is the probability of the cost occurring in a 24 hour time period, $\bar{f}_i$ is the associated cost above the baseline value at the given penetration without the FW function, i.e., $\bar{f}_i = f_i(FOM) - f_i(FOM_0)$.

The price of electricity in Lanai was selected to be 0.448 $/kWh based on the price of electricity for a residential customer on Lanai who uses up to 250 kWh of energy per month [27]. This corresponds to the incurred cost (due to lost net metering revenue) of a residential homeowner curtailing to provide the frequency reserve. P_1=1 because E_{loss} represents an average 24 hour time period.

The f_{min_f} term was included to account for unserved load costs. As of 2014, the Hawaiian Electric Company (HECO) implements blocks of underfrequency load shedding (UFLS) with Stage 1 occurring at 58.7 Hz, Stage 2 at 58.5 Hz, and Stage 3 at 58 Hz [28], although, the UFLS relay trip points will be adjusted with higher penetration levels. The P_2 coefficient is the probability of the N-1 contingency occurring in a 24 hour period. Previously, Sandia analyzed HECO and Maui Electric Company (MECO) frequency data to determine the number and magnitude of over- and under-frequency events [29]. Using 2011 as a baseline, MECO experienced 12 underfrequency events below 59.5 Hz (with 1 below 58.5 Hz), so P_2 was selected to be 12/365 = 0.033 to represent the probability of a grid disturbance.

The cost of lost load can be calculated in different ways, but Lawrence Berkeley National Laboratory (LBNL) and Department of Energy (DOE) created a simple Interruption Cost Estimate (ICE) calculator to estimate the economic losses given the duration and severity of the blackout [30]. Here, it was assumed that 3,000 people on Lanai Island were residential customers, 200 were commercial and industrial, and the load was lost for 60 minutes. The percentage of the customers affected by the outage is linearized between 58.7 Hz Stage 1 UFLS and bulk collapse at 57 Hz—in part because PV frequency ride-through settings were recently widened to allow normal operation down to 57 Hz [31]. Based on these assumptions, cost is modeled as

$$f_2\left(f_{\min\_f}\right) = \begin{cases} 0 & for \quad f_{\min\_f} > 58.7 \\ P_b\left(\dfrac{58.7 - f_{\min\_f}}{1.7}\right) & for \quad 57.0 \le f_{\min\_f} \le 58.7 \\ P_b & for \quad f_{\min\_f} < 57.0 \end{cases} \quad (2)$$

where the price for a complete blackout is calculated as P_b = $253.5k given the above values and default ICE Hawaiian demographic information.

Power plants experience additional wear when they are operated at larger ramp rates. The O&M costs for cycling the Lanai diesel generators is unknown, but previous work with coal and gas power plants indicate that the costs for doubling the diesel generator power ramp rate will increase the associated cycling costs by a factor of up to 10 [32]. When gensets operate with proportional droop control and there is an increase in the rate of variation of the grid frequency, the generator ramp rates will increase roughly proportionally and inflict a greater creep and fatigue damage. Assuming genset replacement costs are $0.38/W and are incurred after 20,000 hrs (2.28 yrs) [22], the replacement costs for the 1.2 MW gensets on Lanai, for example, are $548/day. Herein, a candidate methodology is considered wherein it is assumed the severity of frequency deviation may be represented by frequency standard deviation and that there will be an additional 300% wear on the genset components when the grid frequency standard deviation doubles from the 20% baseline, such that:

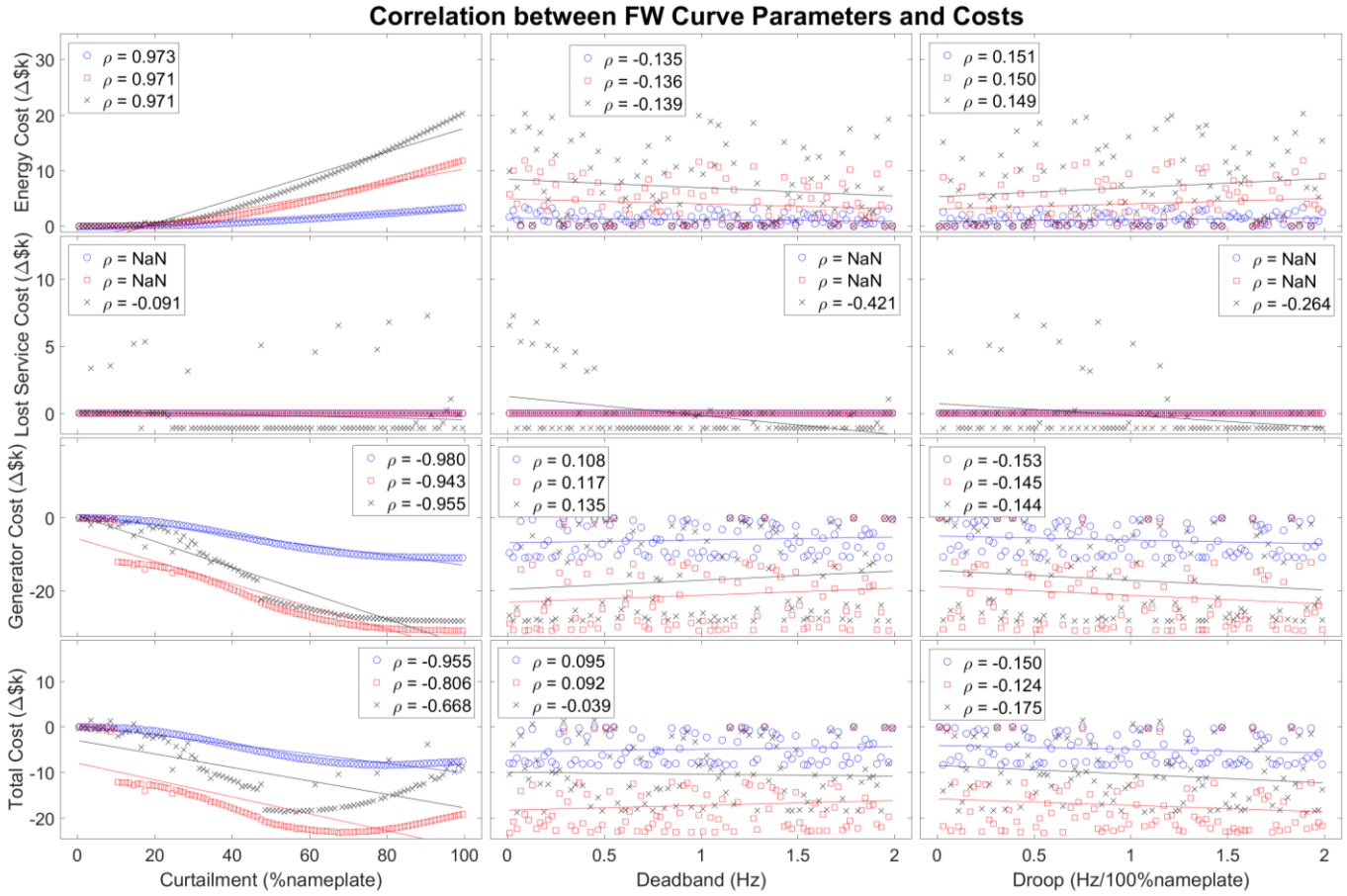

Fig. 5. FW parameter influence on costs for 20% (blue), 70% (red) and 120% (black) penetration cases.

$$f_3(\sigma) = P_{gen} \cdot C\left[1+3\left(\frac{\sigma-\sigma_{0\_20\%}}{\sigma_{0\_20\%}}\right)\right] \quad (3)$$

where C is the replacement cost per watt and P_{gen} is the diesel power capacity interconnected to the system [19].

Using the Latin Hypercube Sampling results, the influence of each parameter on the costs is depicted in Fig. 5. As seen in the results, there are FW functions that result in utility cost savings for all penetration scenarios; specifically, there are minima in the curtailment values for each penetration level. The smaller deadbands produce slightly greater cost savings, but the droop has little influence on the total utility cost. As PV penetration increases from 20% to 70%, the utility would save more money from implementing the FW function, seen in the minimum LHS cost for each penetration level in Table I.

At lower penetrations, the cost function favors deeper curtailment levels. This may seem counterintuitive, but there is significantly less revenue loss at lower curtailment levels and FW implementation extends the genset life by smoothing the day-long frequency results. In general, the optimal curtailment figures can be attributed to a high estimated cost of generator wear. At low penetrations, more diesel gensets are connected to the grid, so the optimal curtailment is higher to mitigate PV variability and provide headroom for control action that reduces generator wear. At higher penetrations, the best curtailment value decreases since energy loss is higher and not offset by reduction in generator wear.

V. Optimization

The PSLF and MATLAB models were wrapped in multiple optimization routines to determine the FW curve that would provide the greatest savings to the utility. The problem is in the form of:

$$\min_{\mathbf{x}} f(\mathbf{x}) \quad s.t. \quad \begin{cases} 0.002 \le x_1 \le 1.000 \\ 0.002 \le x_2 \le 2.000 \\ 0.002 \le x_3 \le 2.000 \end{cases} \quad (4)$$

where $f(\mathbf{x}) = P_1 \cdot \bar{f}_1(E_{loss}(\mathbf{x})) + P_2 \cdot \bar{f}_2(f_{\min\_f}(\mathbf{x})) + P_3 \cdot \bar{f}_3(\sigma(\mathbf{x}))$ and $\mathbf{x} = [x_1, x_2, x_3]$ and x_1 is the curtailment, x_2 is deadband, and x_3 is the droop. The optimization routine was executed in MATLAB, and the principle components are illustrated in Figure 6.

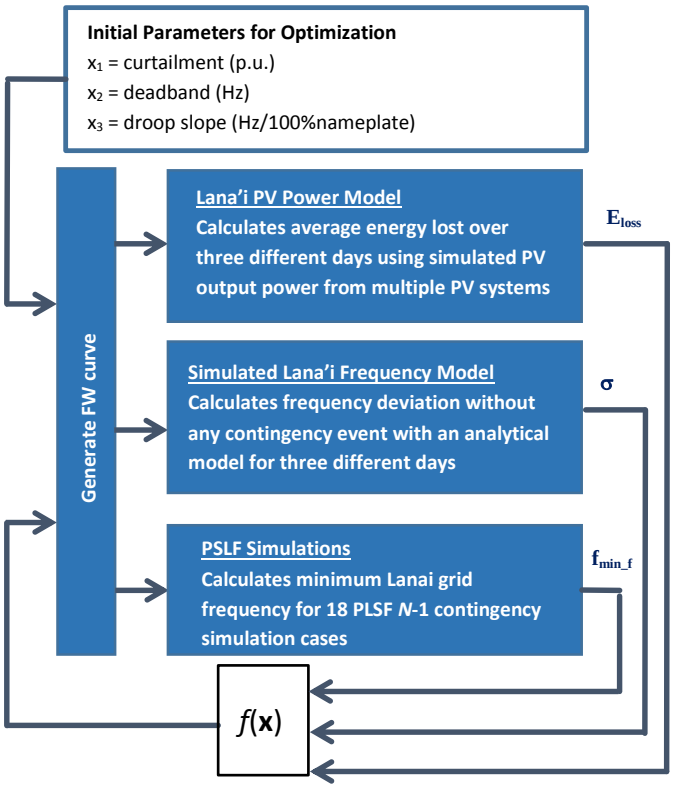

Figure 6: Optimization loop with MATLAB and PSLF models and associated figures of merit.

Initially, the optimization was attempted using the sequential quadratic programming (SQP) routine in MATLAB with the initial starting point at the best LHS result for each penetration level. Since there were no nonlinear equality or inequality constraints in the SQP optimization problem, the algorithm approximated Newton's method to find the optimal FW curve. The SQP optimizer found a nearly identical FW curve compared to the best LHS. This is due to weak cost correlations for the deadband and droop parameters and, likely, from local minima in the fitness landscape. In order to improve the optimization results, a second optimization routine called the interior point method was used to determine the optimal FW curve. Again, the starting point was selected to be the best LHS result. As shown in Table 1, the interior point method resulted in slightly better solutions than the LHS data and the SQP method for the 70% and 120% penetration cases.

As can be seen in the results in Table I, all the methods found similar curtailment values for each of the penetration levels, but there were discrepancies regarding the optimal droop values. When comparing the cost values, it is clear that deadband and droop are secondary influences on the FOMs and cost function, so they do not heavily influence the revenue from FW implementation. That is to say that the inconsistencies between LHS, SQP, and interior point are due to the low sensitivity of the cost model to changes in deadband and droop, and therefore influenced by the starting point of the SQP and Interior Point algorithms. The weak influence of the deadband and droop on the total cost is good news for HECO and other utilities, because these low-sensitivity parameters do not need to be set precisely to see near-optimal returns from FW implementation. It is suggested that alternative nonlinear optimization techniques which are resistant to becoming trapped in local minima (e.g., genetic algorithms, ant colony optimization, and particle swarm optimization) should be investigated for the FW function parameter optimization problem.

VI. CONCLUSIONS

When appropriately programmed, the IEC 61850-90-7 frequency-watt function is capable of providing contingency reserves and frequency regulation. These benefits are dependent on the availability of PV power, but as PV generation displaces traditional generators and reduces system inertia, photovoltaic inverters must participate in grid operations as frequency regulation and primary frequency reserves. The FW function reduces the variability of the PV power by curtailing the power and provides headroom to respond to contingency events.

In this work, we investigated the influence of the FW function on the Lanai, HI electricity grid in its current state with 20% PV penetration and in possible future configurations of 70% and 120% PV penetration. High-fidelity models were developed in MATLAB and PSLF to provide a complete representation of the island grid's response to PV variability and to faults and loss of generation in each configuration. These real-world models and scenarios were used in simulation efforts that clarified how the FW function affects the dynamics of the system, and they were used in optimization schemes to show how best to make money using the FW functions. The results showed

TABLE I. LOWEST COST LHS AND OPTIMIZATION RESULTS

Penetration	Technique	Curtailment (%)	Deadband (Hz)	Droop (Hz/100%nameplate)	Cost (Δ$k/day)
20%	LHS	78.50	1.730	1.610	-8.35
	SQP (76 Steps)	78.89	1.681	1.566	-8.35
	Interior Point (203 Steps)	78.91	1.733	1.622	-8.35
70%	LHS	67.50	0.010	0.551	-23.22
	SQP (147 steps)	67.50	0.010	0.551	-23.22
	Interior Point (77 Steps)	67.11	0.002	0.416	-23.30
120%	LHS	56.50	0.050	1.910	-18.78
	SQP (78 steps)	56.50	0.050	1.910	-18.78
	Interior Point (128 Steps)	47.70	0.042	0.004	-20.43

implementation of the FW function could immediately save HECO money even if they paid PV owners for the lost generation opportunity costs. Additional cost savings are available in the 70% and 120% PV penetration scenarios. This is a significant finding because it shows that the implementation of advanced grid functions does not only provide technical grid support, but is also economical when implemented with the proper settings. It is anticipated this will be the case for other regions and jurisdictions in the US and the world, and the models and method of analysis can be extended to these areas to find the optimal FW settings; although the cost function could be expanded to include other expenses and the models for energy loss, lost load, and generator replacement costs could be improved.

Using Latin Hypercube Sampling, 100 FW curves were generated and compared with numerical simulations of fault and non-event cases. For each FW definition, simulations of three penetration levels were conducted for (a) six PSLF simulations representing three times of the day and two fault scenarios and (b) three full day simulations of different irradiance conditions to estimate lost PV generation revenue and non-event frequency variability. Based on six figures of merit and a cost analysis, the tradeoffs of different FW curve parameters were investigated.

The proposed methodology is promising for the development of cost estimates when implementing FW functions, but future work should be conducted to refine and validate the cost model. It should also be noted that autonomous FW functions can be programmed into energy storage systems (ESSs) to provide similar capabilities—as currently required in Italian and German interconnection requirements [11]. Furthermore, HECO has requested ESSs with FW capabilities in the Oahu Energy Storage System RFP [33]; so, a similar FW function analysis should be performed for ESSs.

Overall, the project successfully established a technique for finding the most economical FW curve for a region. This method can be adopted by utilities in CA, HI, and elsewhere in the world to pick desirable FW settings. As more inverters are programmed with advanced grid support functions, they will increasingly become a major component of ancillary service strategy. Deployment of advanced interoperable inverters also opens the door for aggregations to provide ancillary services. These "virtual power plant" (VPP) aggregations can be programmed to support grid frequency and voltage and also respond to grid disturbances, such as an *N*-1 contingency. In this paper, a VPP-like aggregation of PV resources was able to smooth the grid frequency during non-contingency periods and also prevent bulk system collapse during an *N*-1 contingency by quickly injecting active power into the grid. In the future, VPPs can be constructed of diverse DER resources and designed to provide a range of services for utilities, ISOs, and RTOs. The economic incentive for utilities to do this was shown in this paper, but third party VPPs could also take advantage of this revenue stream by providing these capabilities and operating in ancillary service and energy markets.

VII. References

[1] J. Leong, C. McMillan, "Governor Ige signs bill setting 100 percent renewable energy goal in power sector," Press Release, Governor of the State of Hawaii, 8 Jun. 2015.

[2] R. Bründlinger, "Grid Codes in Europe for Low and Medium Voltage," 6th International Conference on Integration of Renewable and Distributed Energy Resources, Kyoto, 18 November, 2014.

[3] Pacific Gas and Electric Company, Electric Rule No. 21, Generating Facility Interconnections, Filed with the CPUC on 20 Jan, 2015.

[4] California Public Utilities Commission, "Recommendations for Updating the Technical Requirements for Inverters in Distributed Energy Resources," Smart Inverter Working Group, Jan 2014.

[5] CEI, *Technical Rules for the Connection of Active and Passive Users to the LV Electrical Utilities*, CEI Reference 0-21, December 2013.

[6] VDE Reference VDE-AR-N 4105, August 2008.

[7] *IEC Technical Report 61850-90-7*, Edition 1.0, Feb 2013.

[8] SunSpec Alliance, SunSpec Specifications & Information Models, Accessed October 2015, URL: http://sunspec.org/download-sunspec-specifications/.

[9] J. Nunneley, et al, "Applying SunSpec Modbus to Meet California Rule 21 Requirements," EPRI Report 3002004696, October, 2014.

[10] J. Johnson, et al., "Collaborative Development of Automated Advanced Interoperability Certification Test Protocols For PV Smart Grid Integration," EU PVSEC, Amsterdam, 22-26 Sept, 2014.

[11] D. Rosewater, et al., International development of energy storage interoperability test protocols for renewable energy integration, EU PVSEC, Hamburg, Germany, 14-18 Sept, 2015.

[12] J. Johnson S. Gonzalez, M.E. Ralph, A. Ellis, and R. Broderick, "Test Protocols for Advanced Inverter Interoperability Functions–Appendices," Sandia Technical Report SAND2013-9875, Nov. 2013.

[13] R. Bründlinger, et al., "Lab Tests: Verifying That Smart Grid Power Converters Are Truly Smart," IEEE Power and Energy Magazine, vol.13, no.2, pp.30-42, March-April 2015.

[14] A. Hoke, D. Maksimovic, "Active power control of photovoltaic power systems," 2013 1st IEEE Conference on Technologies for Sustainability (SusTech), pp.70-77, 1-2 Aug. 2013.

[15] C. Rahmann and A. Castillo, "Fast frequency response capability of photovoltaic power plants: The necessity of new grid requirements and definitions," Energies, vol. 7, no. 10, pp. 6306-6322, 2014.

[16] P.P. Zarina, S. Mishra, P.C. Sekhar, "Deriving inertial response from a non-inertial PV system for frequency regulation," IEEE PEDES, Karnataka, India, 16–19 December 2012.

[17] A. Oudalov, D. Chartouni, C. Ohler, "Optimizing a Battery Energy Storage System for Primary Frequency Control," IEEE Transactions on Power Systems, vol.22, no.3, pp.1259-1266, Aug. 2007.

[18] M. R. Aghamohammadi, H. Abdolahinia, A new approach for optimal sizing of battery energy storage system for primary frequency control of islanded Microgrid, JEPE, no. 54, pp. 325-333, Jan 2014.

[19] J. Neely, S. Gonzalez, J. Delhotal, J. Johnson, M. Lave, Evaluation of PV Frequency-Watt Function for Fast Frequency Reserves, IEEE APEC, Long Beach, CA, March 20-24, 2016.

[20] M. D. McKay, R.J. Beckman, W.J. Conover, "A Comparison of Three Methods for Selecting Values of Input Variables in the Analysis of Output from a Computer Code", Technometrics, vol. 21, no. 2, pp. 239–245, May 1979.

[21] J. Johnson, et al., "Initial operating experience of the La Ola 1.2 MW photovoltaic system," Sandia Technical Report SAND2011-8848,2011.

[22] B. Kroposki, et al., Integrating High Levels of Renewables into the Lanai Electric Grid, Tech. Report NREL/TP-5500-50994, June 2012.

[23] M. Lave, J. Kleissl, J. S. Stein, "A Wavelet-Based Variability Model (WVM) for Solar PV Power Plants," Sustainable Energy, pp. 1-9, 2012.

[24] M. Lave and J. Kleissl, "Cloud speed impact on solar variability scaling – Application to the wavelet variability model," Solar Energy, vol. 91, pp. 11-21, 2013.

[25] M. Lave and J. Kleissl, "Testing a wavelet-based variability model (WVM) for solar PV power plants," IEEE PES General Meeting, 2012.

[26] M. Lave, J. Kleissl, and J. S. Stein, "A Wavelet-Based Variability Model (WVM) for Solar PV Power Plants," IEEE Transactions on Sustainable Energy, 2013.

[27] Maui Electric Company, Ltd. Lanai Division, Schedule "R" Residential Service, Decision and Order No. 31288, Filed May 31, 2013.

[28] Maui Electric Company, Ltd., Maui Electric Power Supply Improvement Plan, Docket No. 2011-0092, Filed 26 Aug, 2014.

[29] C.A. Silva Monroy, V.W. Loose, Hawaii Electric System Reliability, Sandia Technical Report, SAND2012-3862.
[30] Interruption Cost Estimate (ICE) Calculator, accessed 23 Oct, 2015, available: http://www.icecalculator.com/index.html.
[31] Hawaiian Electric Companies, Transient Over-Voltage and Frequency & Voltage Ride-Through Requirements for Inverter–Based Distributed Generation Projects, June 2015.
[32] N. Kumar, P. Besuner, S. Lefton, D. Agan, and D. Hilleman, Power Plant Cycling Costs, NREL Report, NREL/SR-5500-55433, July 2012.
[33] O'ahu Energy Storage System Engineering, Procurement and Construction (EPC) Request for Proposal, RFP 072114-01, July 2014.

VIII. BIOGRAPHIES

Jay Johnson (M'12) is a senior member of technical staff at Sandia National Laboratories and has been researching renewable energy and energy efficiency systems for more than 10 years. Jay leads a number of multidisciplinary, renewable energy research projects including the coordination of the Smart Grid International Research Facilities Network (SIRFN) advanced inverter interoperability test protocol development and the virtual power plant program at Sandia National Labs.

Jason C. Neely (M'03) is a principal member of technical staff at Sandia National Laboratories. He received B.S. & M.S. degrees in Electrical Engineering from the University of Missouri-Rolla in 1999 and 2001 respectively. From 2001-2007, he worked at Sandia National Labs in the Intelligent Systems & Robotics Center. Jason later received his Ph.D. in Electrical and Computer Engineering at Purdue in 2010 for development of new control techniques for power electronics. Since 2010, Jason has been a researcher at Sandia National Labs focusing on grid integration of power electronic based renewable energy sources and energy storage systems.

Jarod Delhotal is a member of technical staff at Sandia National Laboratories in the Electrical Science and Experiments Department.

Matthew Lave received the Ph.D. degree in aerospace engineering from the University of California, San Diego. He is a Senior Member of the Technical Staff at Sandia National Laboratories, working in the Photovoltaic and Distributed Systems Integration Department. His specialty areas are solar resource assessment, PV performance monitoring, and grid integration of PV, especially related to large data set analysis. He currently develops and validates models of solar irradiance, spatial smoothing of solar variability across large PV plants, and the impact of PV to the electric grid.